nature portfolio

https://doi.org/10.1038/s41551-022-00876-4

Supplementary information

Prospective testing of clinical Cerenkov luminescence imaging against standard-of-care nuclear imaging for tumour location

In the format provided by the authors and unedited

Contents

Supplementary Figures

1. Detection uniformity and enclosure light tightness
2. Characterizing the isotope sensitivity of the CLI system
3. Sensitivity determination of CLI fiberscope using a calibrated source
4. Resolution performance of CLI system with binning
5. *In vivo* testing of the CLI system linearity and filter performance
6. Reduction of gamma strike scintilation and effectiveness of lead shielding, also alpha emitter imaging
7. Phantom preparation and imaging for testing of CLI device
8. System sensitivity to angular incidence
9. Tumor depth phantom for depth analysis with optical filters
10. Intensity analysis of $^{223}RaCl_2$ patients
11. Schematic of patient CLI post processing
12. CLI signal response by distance

Supplementary Methods

References

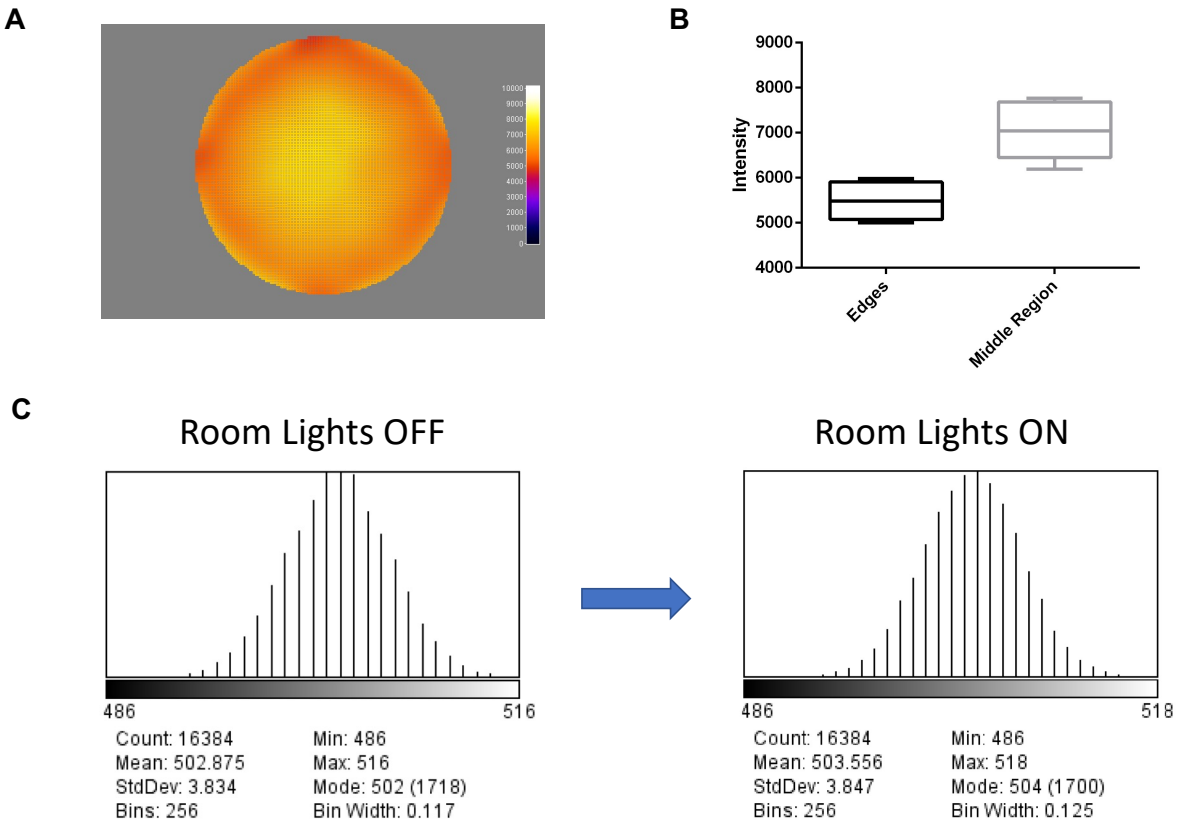

Supplementary Fig. 1 | Detection uniformity and enclosure light tightness. a, Surface CL plot of uniformly distributed ^{68}Ga in a petri dish in the preclinical enclosure and **b**, quantified signal changes on edges and middle regions of the ^{68}Ga petri dish. **c**, Histogram showing background signal intensity of the clinical enclosure with room light off vs on indicating the enclosure is light proof. Box plot in **b** represents pixel values obtained from the petri dish image with central line as median, and box edges as upper and lower quartiles

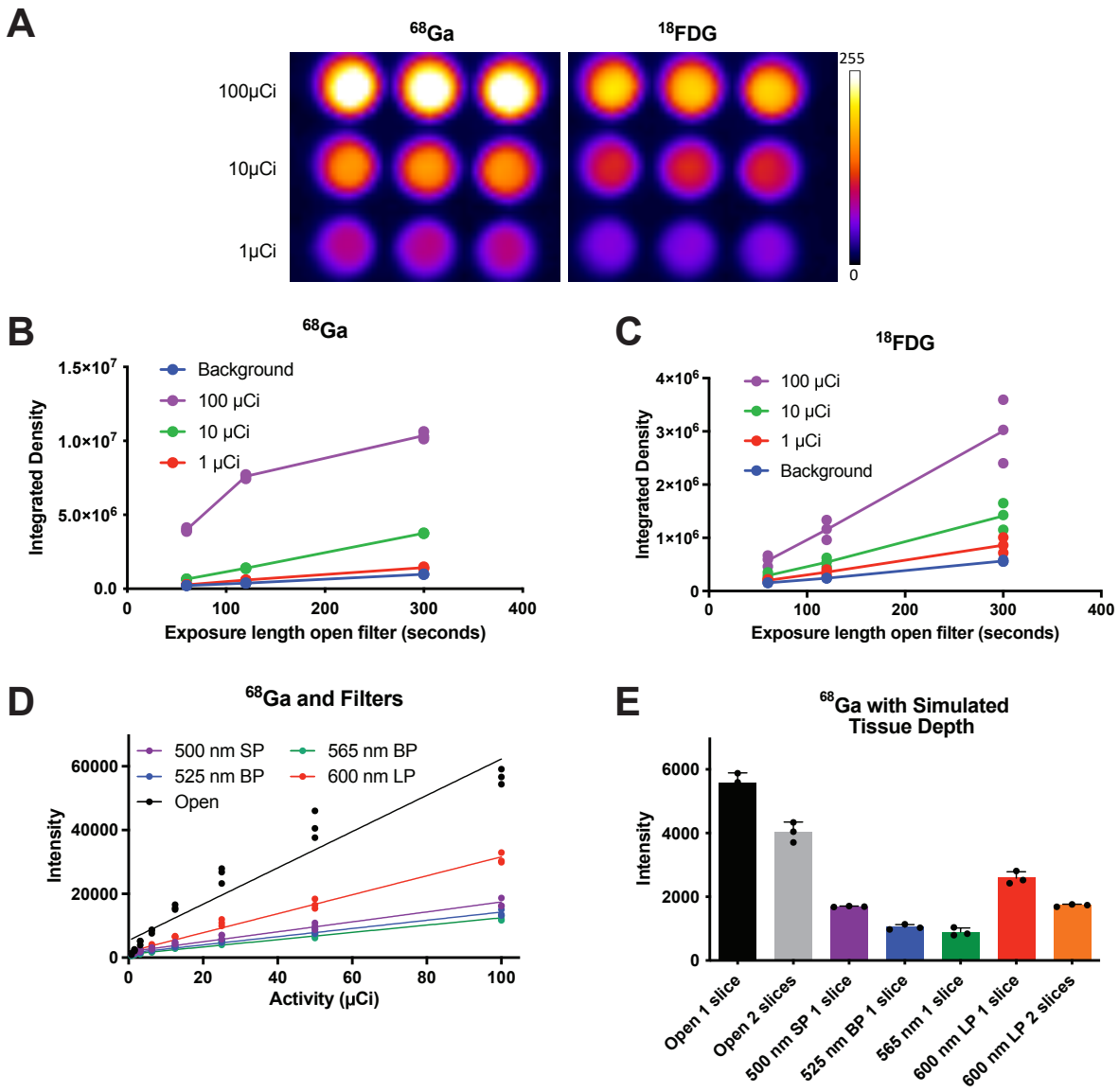

Supplementary Fig. 2 | Characterizing the isotope sensitivity of the CLI system. a, CL images of ^{18}F-FDG and $^{68}GaCl_3$ **b**, CL response of $^{68}GaCl_3$ to varying exposure set to 4x4 binning **c**, CL response of ^{18}F-FDG to varying exposure **d,** CL response of $^{68}GaCl_3$ to varying amounts of activity. **e,** CL response of $^{68}GaCl_3$ to bologna slices. For **b-e,** n=3 technical replicates per activity concentration. For **e,** n=3 technical replicates with 100μCi ^{68}Ga for bologna slices and filter measurement. All data points shown with bars representing the mean and error bars defining the SEM.

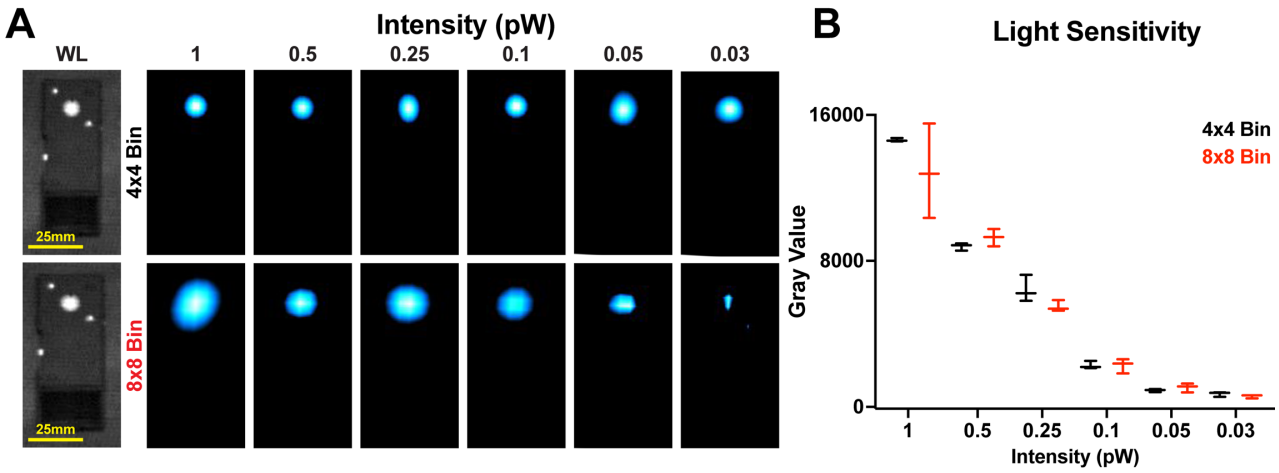

Supplementary Fig. 3 | Sensitivity determination of CLI fiberscope using a calibrated source. **a**, White light and EMCCD mode (for Cerenkov imaging) showing the CLI fiberscope system can detect light down to 0.03 pW. Calibrated light source (L11494-660, Hamamatsu, Japan) was set at 1.0 pW with a series of neutral density filters (NE-503B-A,506B-A,510B-A,513B-A,551B-A each housed in a respective LMR05 mount, Thorlabs, NJ, USA) applied to measure the lower intensities and measured with 4x4, and 8x8 binning. **b,** Quantification of images in **a** showing similar intensity between 4x4 and 8x8 binning modes with a plateau near 0.03 pW. Box and whisker plots showing min to max of n = 3 technical replicates per respective measurement with the middle line corresponding to the median value with error bars defining the SEM.

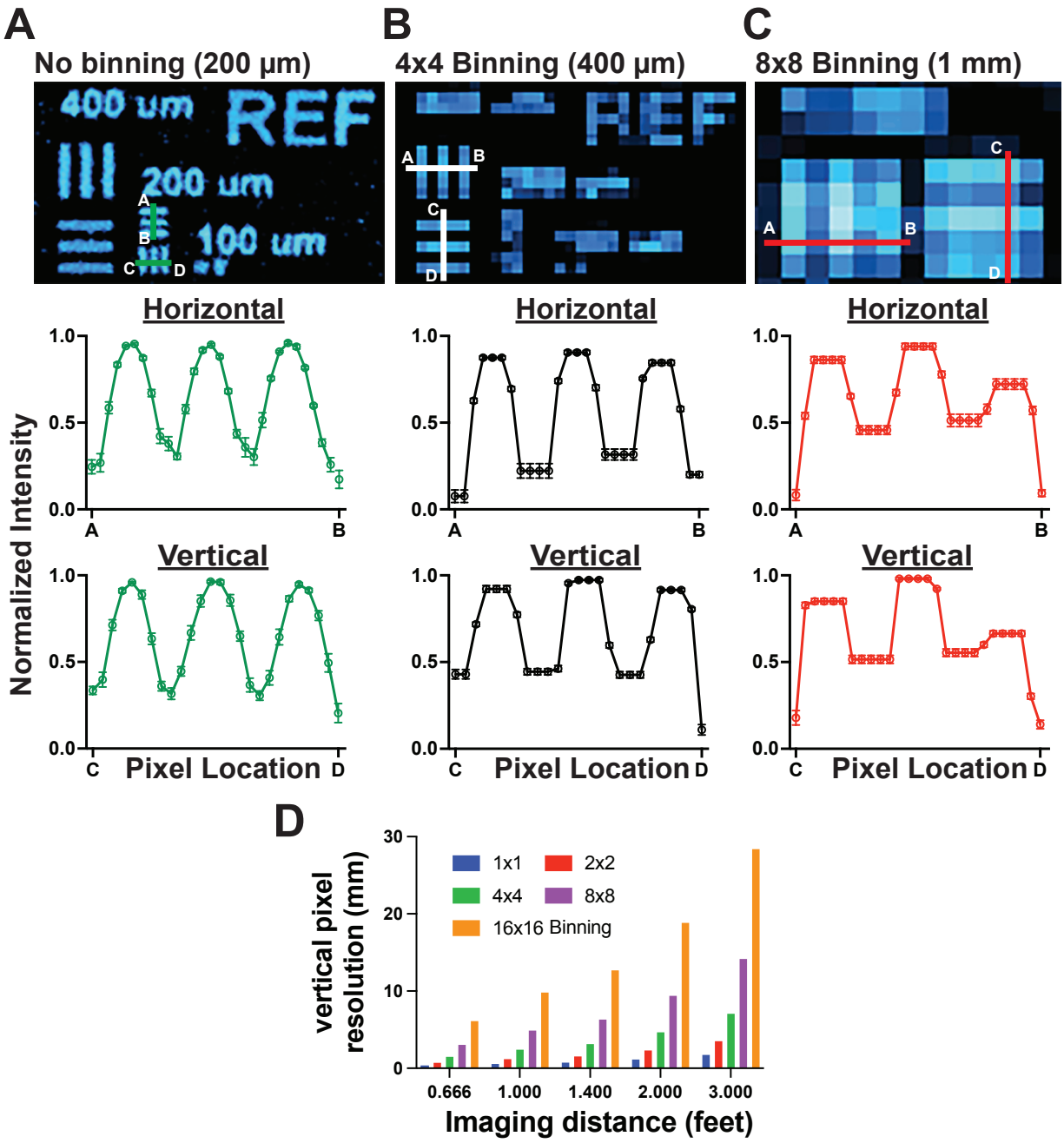

Supplementary Fig. 4 | Resolution performance of CLI system with binning. Top, images of a luminescent resolution test target developed by LightPoint based on the USAF 1951 resolution targets (Sighting Block B, LPA_00699_B) placed at 15 cm (0.666 feet) from the camera with **a,** no binning applied, **b,** 4x4 binning, and **c,** 8x8 binning. Middle, horizontal resolution determination for each binning mode. Bottom, vertical resolution determination for each binning mode. Respective normalized intensities show partial loss of trough definition with binning but retain the overall pattern, each graph represents the mean with SEM for n = 7 technical replicates for each line of measured pixels. The max possible resolution is defined in both the horizontal and vertical as 200 μm for no binning, 400 μm for 4x4 binning and 1 mm for 8x8 binning. **d,** CL images were acquired for patients at a greater distance, typically ~43cm with a resolution of ~3mm per pixel with final image processing including smoothing steps, further reducing the CL resolution.

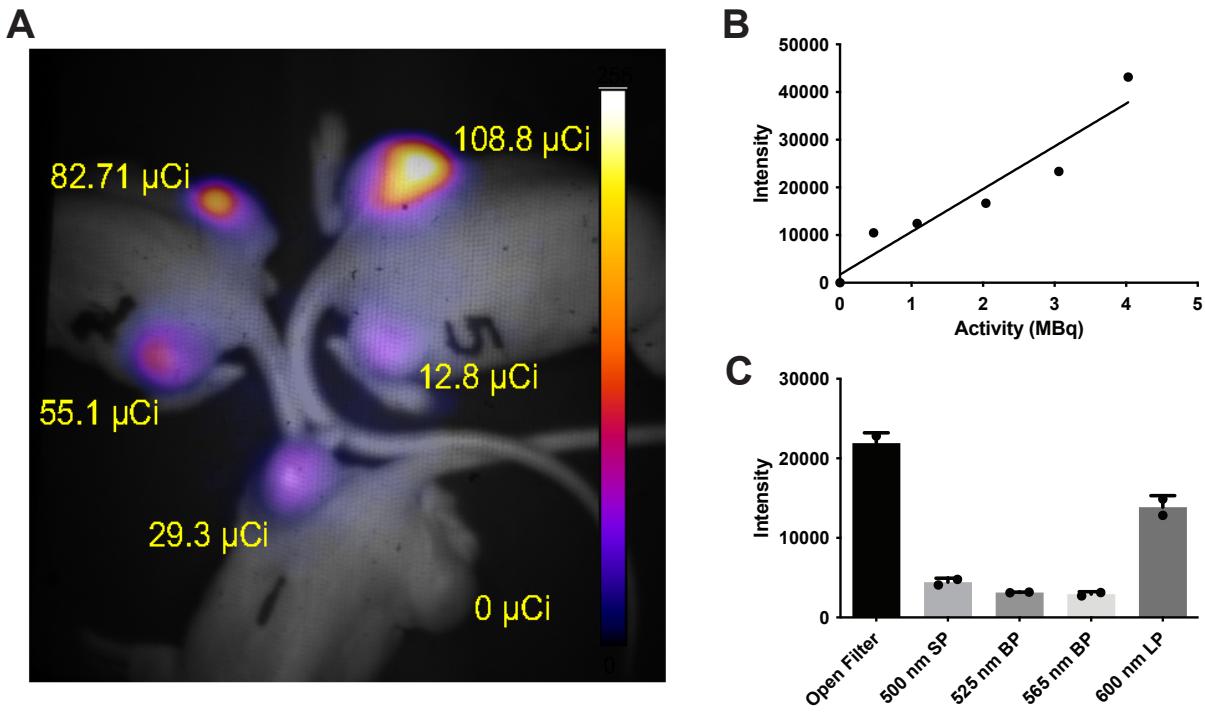

Supplementary Fig. 5 | *In vivo* testing of the CLI system linearity and filter performance. **a,** CL image of nude mice bearing HT1080 tumors with increasing amounts of intratumorally injected ^{18}F-FDG. **b,** CL response to ^{18}F-FDG activity at the tumor site of mice imaged in **a**. **c,** CL response to different optical filters for n=3 separate mice intratumorally injected with 30μCi (1.11MBq) $^{68}GaCl_3$. Graph in **c** represents mean with error bars representing SEM.

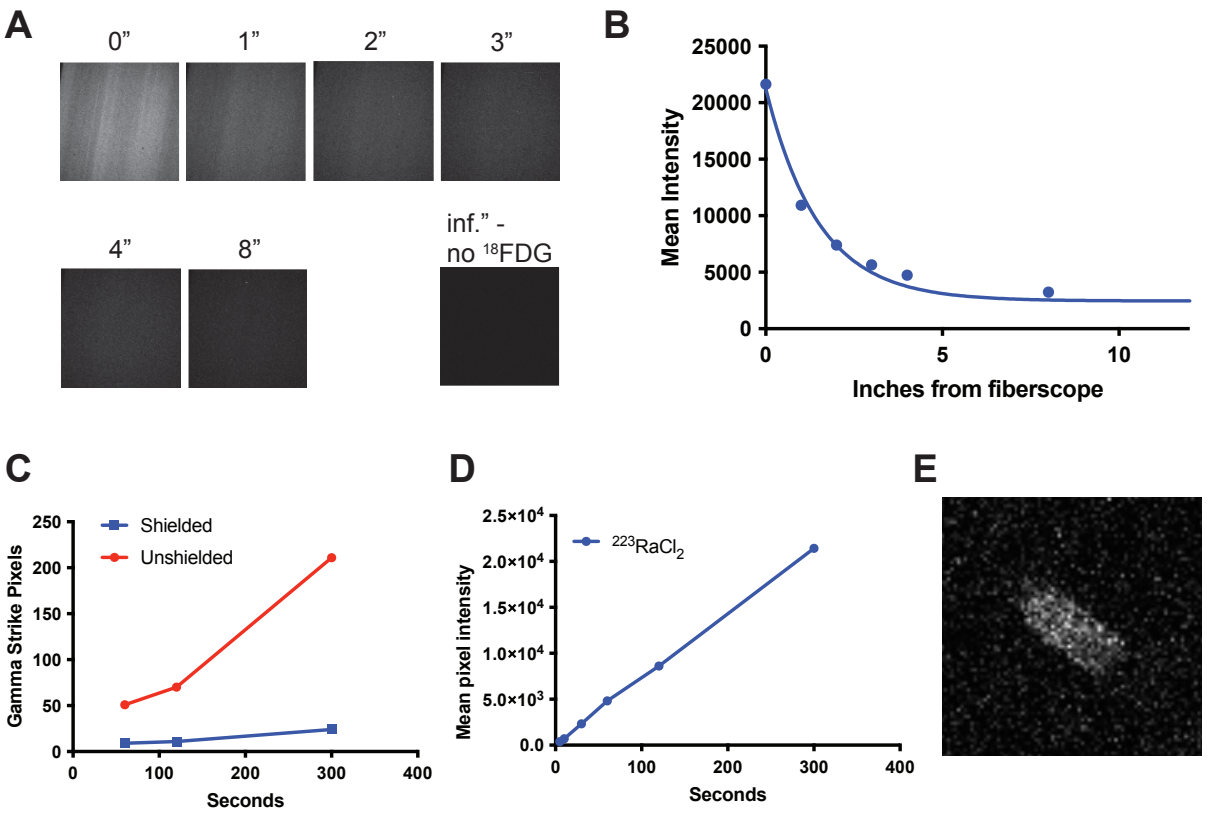

Supplementary Fig. 6 | Reduction of gamma strike scintilation and effectiveness of lead shielding, also alpha emitter imaging. a, Fiber scintillation images where an ^{18}F-FDG source was placed at increasing distances next to the fiber, with the lens covered. **b,** Mean pixel intensity of scintillation images in **a** plotted as a function of distance. **c,** Effect of installed lead shield on preventing gamma strikes to EMCCD sensor. Implementation of the Fast Fourier Transform during image post processing removed spurious light signal other than CLI. **d,** Recorded intensities for $^{223}RaCl_3$ at varying exposure times. **e,** Image of 37μCi $^{223}RaCl_3$ in 6mL syringe as detected by the system after 5 second exposure. Data points in **b-d** are single experiments with a single phantom.

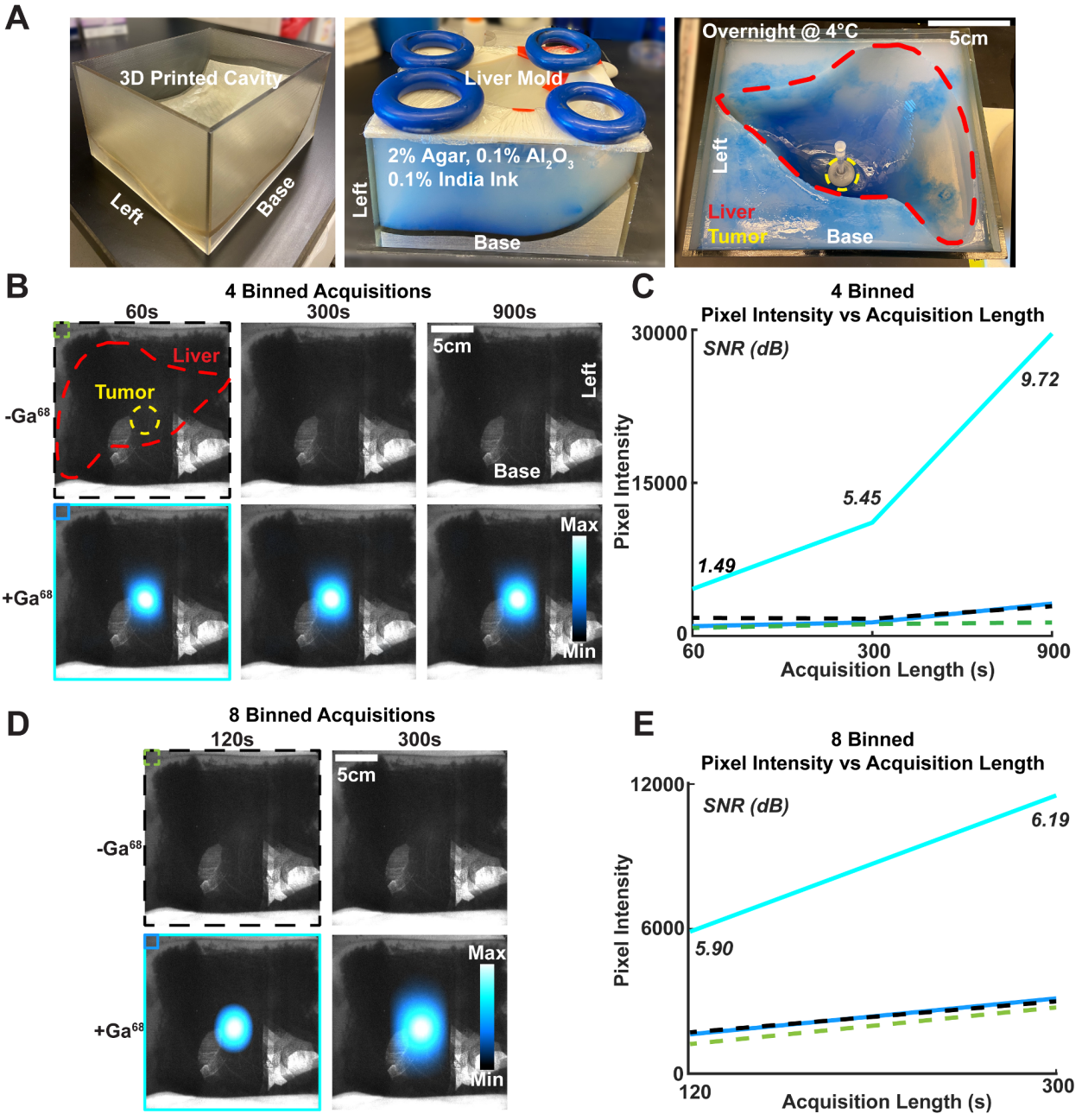

Supplementary Fig. 7 | Phantom preparation and imaging for testing of CLI device. a, Left, the empty 3D printed cavity to be filled with tissue mimicking agar. Middle, the filled cavity including liver mold with tumor divot (not visible). Weights are added to ensure the mold is fixed in place. Right, left overnight at 4°C to solidify the liver mold was removed leaving a liver shaped cavity and lesion divot. A 3D printed sphere was then filled with ^{68}Ga and placed into the divot highlighting a tumorous lesion on the liver. **b,** Images showing the resulting 4x4 binned images for varying acquisition lengths with and without ^{68}Ga. Cerenkov Luminescence was readily detected in the presence of 0.5 mCi ^{68}Ga. **c,** Corresponding max pixel intensity values for the regions of interest as highlighted by the dotted and solid lines in **b**. SNR values are shown in italics in dB. **d,** Images from the 8 binned acquisitions under the same conditions as 4 binned images. The 300s acquisition appears more scattered in comparison to its 4 binned counterpart, likely due to the lower resolution from increased binning. **e,** Corresponding max pixel intensity values as from the regions of interest shown in **d**. SNR values are shown in italics in dB. Similar pixel values are shown for both 4 and 8

binned imaging modes whilst the increase in dark noise for 8x8 binned images at 300s slightly reduces the SNR. In all cases ^{68}Ga images are thresholded respectively and pixel intensity values have been corrected to account for ^{68}Ga decay. SNR values in **c** and **e** are extracted from single images taken every 300 seconds with and without ^{68}Ga under 4x4 binning and 8x8 binning acquisition.

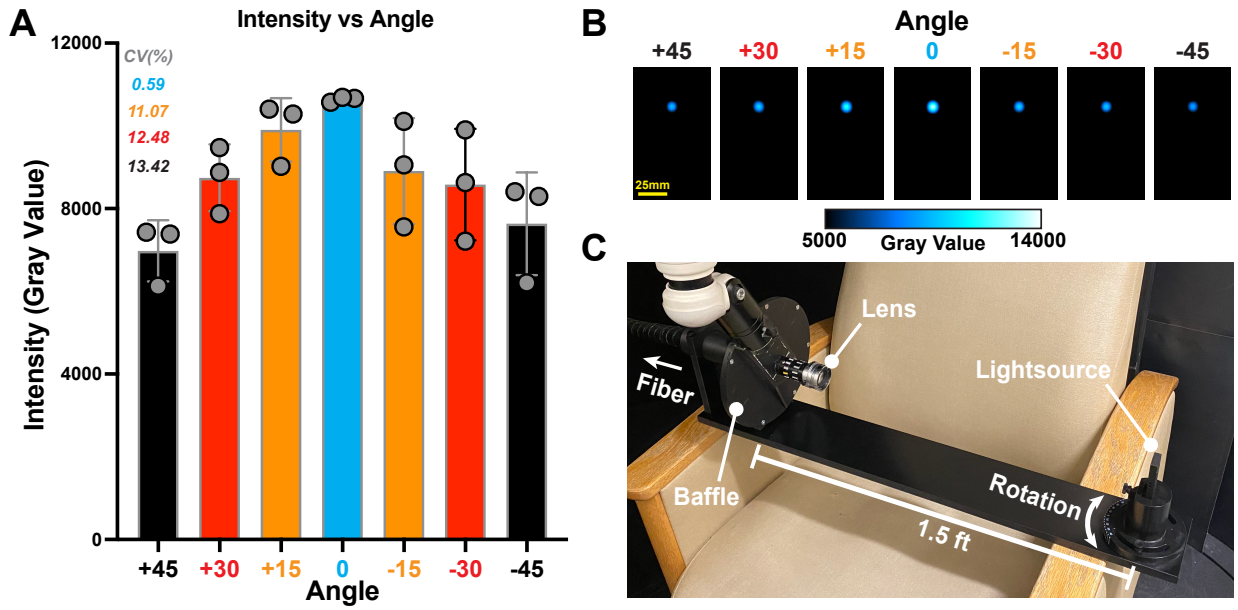

Supplemental Fig. 8 | System sensitivity to angular incidence. a, Recorded gray values versus incidence angle of light for the clinical fiberscope system. Angular sensitivity was tested from +45 to -45 degrees in 15 degree steps in line with orientations used in clinical screening. Coefficients of variance are shown (in percentage) for each angle where n = 6 measurements as a composite of both positive and negative angle rotation and n = 3 for the planar view with 8x8 binning and an exposure time of 5 minutes respectively, with the light source emitting 1 pW at 660nm. Bar represents mean with SEM in gray. Each measurement is represented by a gray dot. **b,** Representative images of the light detected at each incident angle. **c,** Photograph of the incidence angle testing setup. The 3D printed device was attached to the cerrobend baffle before being mounted on the patient chair for support. 3D printed mounts along with a manually rotating stage with 5 degree resolution indications were used to determine the incidence angle.

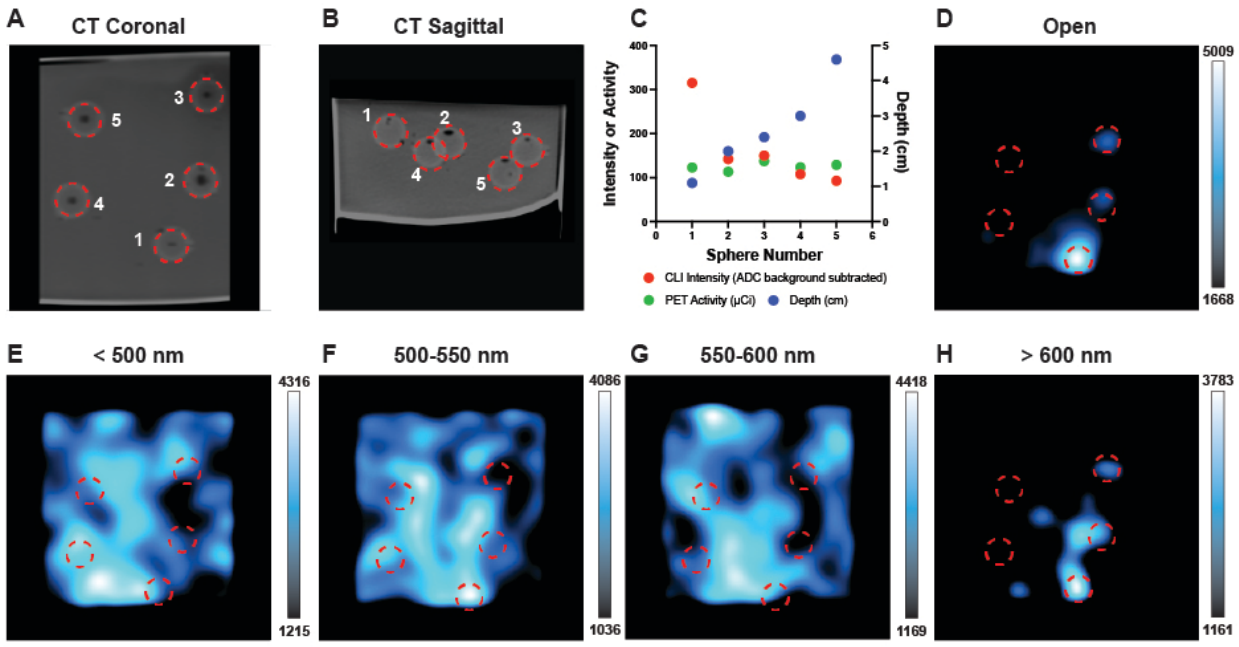

Supplementary Fig. 9 | Tumor depth phantom for depth analysis with optical filters. Five spheres containing ^{18}F-FDG (~570 μCi each) were embedded into an optical phantom comprised of tissue mimicking agarose[1]. **a-b,** CT of tumor spheres were used to determine spacing and depth between spheres, and PET measured 4 hours later to describe **c,** the activity present during imaging and each sphere depth. **d**, Open filter image shows sphere 1 with the highest CLI intensity is the shallowest sphere followed by spheres 2-5 of increasing depth. CLI intensity of the spheres in **d** align with the combination of sphere depth and activity present in the spheres. **e,** short-pass filtering did not recapitulate sphere placement, nor for narrow bandpass images in **f,** and **g**. These filters could not segment light below 600nm due to the high absorption and scattering of light by the phantom at these wavelengths similar to normal tissue, leaving little Cerenkov light to detect within the short-pass and two bandpass filters. However, **h**, long pass filtering above 600nm reproduced a similar image to the open filter with more of spheres 2-5 seen in the image. Here spectral filtering below 600nm was ineffective due to the high degree of absorbed Cerenkov light. However, the 600nm long pass filter provided effective filtering suggesting additional work on longer wavelength filters is warranted, provided the camera efficiency and Cerenkov emission is sufficient.

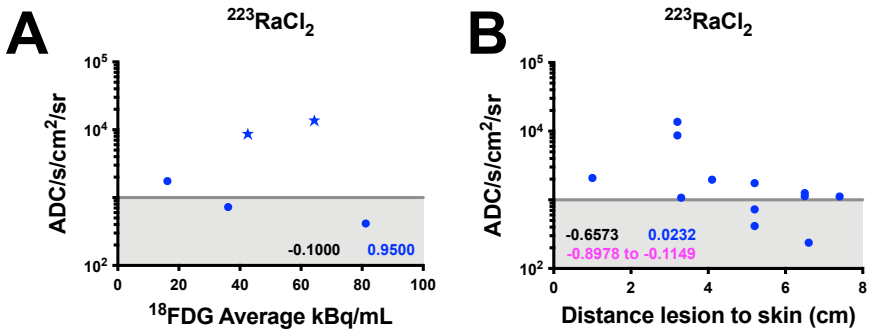

Supplementary Fig. 10 l Intensity analysis of $^{223}RaCl_2$ patients. **a-b,** Intensity analysis was not found to be significant with activity administered, however was significant with lesion depth. Spearman r in black, CI in magenta, and P-Value in blue. **a** n=5 patients with corresponding ^{18}FDG image within 1 month of $^{223}RaCl_2$ injection, **b**, image intensity from n=7 patients with multiple images per patient and location.

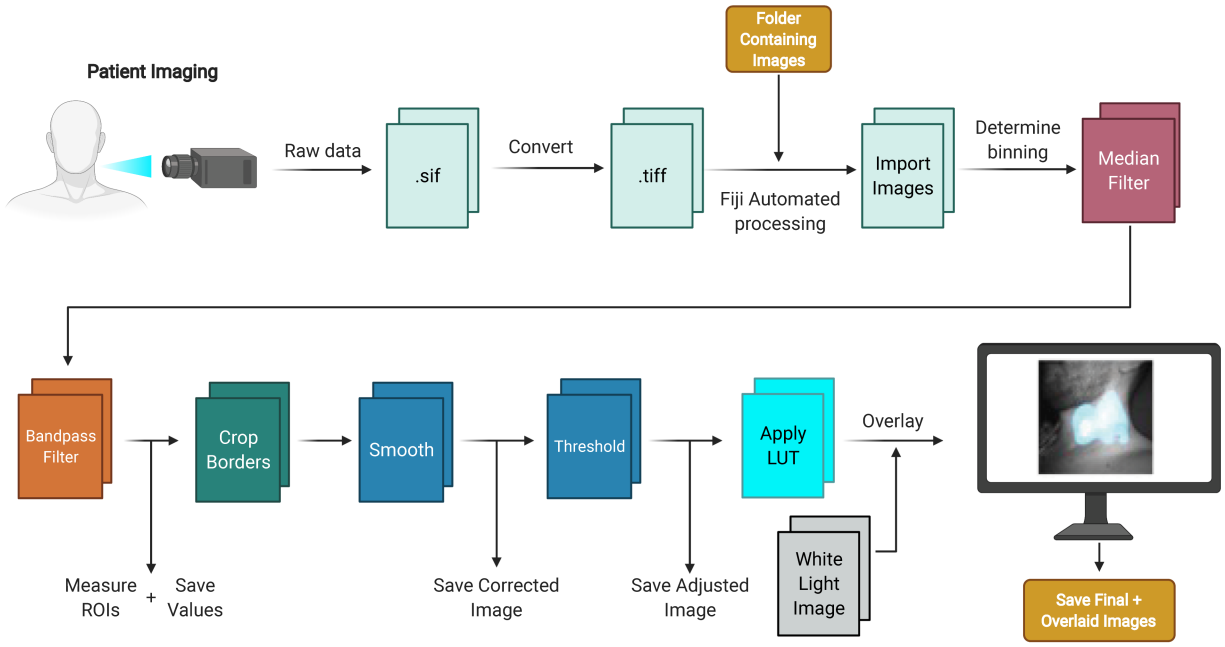

Supplementary Fig. 11 | Schematic of patient CLI post processing. Recorded raw files from the camera were converted to tiff images (Andor, Solis) for automated batch processing in Fiji (ImageJ 2.1.0). A script was written to automatically import images and apply processing steps based on their respective size due to binning (4x4 binning = 128x128 pixels, 8x8 binning = 64x64 pixels). Once imported images were processed to remove gamma strikes (outlier removal via median filtering) along with sensor deformations, vignetting and noise suppression (bandpass FFT). Predetermined regions of interest were then measured and recorded (top left corner region of interest and entire image pixel values). Following this, barrel distortions (vignetting) from the lens edges were removed via border cropping followed by smoothening. Cropping amounts and smoothening levels were binning dependent. Finally, the image was thresholded to 95% of the max signal intensity and the Cyan Hot LUT was applied before being resized and overlaying on the corresponding white light (anatomical) image. Outputting images at various processing steps allowed for future manual adjustment by the user if necessary. Processing was otherwise autonomous with the user only required to select image directories. Figure made with Biorender.com.

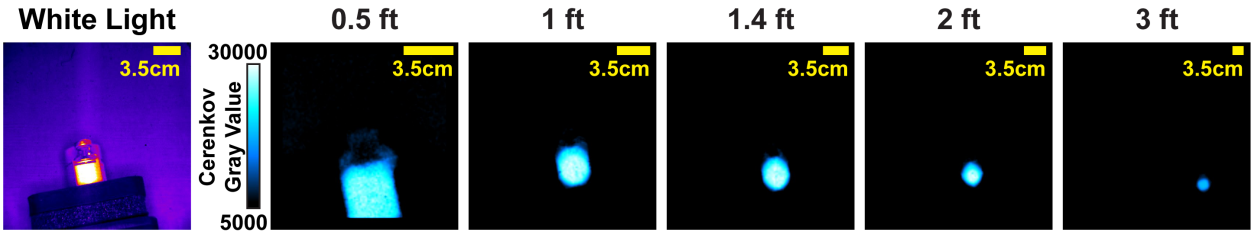

Supplementary Fig. 12 | CLI signal response by distance. A single vial of ^{177}Lu-DOTATATE 200mCi (7.4GBq) was imaged over 60s at various distances between 0.5'-3'. The integrated signal was used to translate signal intensity to a single imaging distance.

Supplementary Methods:

Camera and Fiberscope Design

The iXon Ultra 897 camera was used for both white light and CLI which could record at 512 x 512 pixels at up to 56 frames per second. The camera was cooled to -80 °C using a Peltier thermoelectric cooling module critical for the reduction of dark current and improving the detection limit. Filter wheel housing was equipped with a 5 position 50 mm round filter system containing the following Edmund Optics filters: 1) no filter, 2) 500 nm short-pass OD4, 3) 525 ± 45 nm 93T bandpass, 4) 575 ± 50 nm OD4 bandpass, and 5) 600 nm long pass OD4.

Design of the Enclosure

The small animal enclosure was equipped with a port for isoflurane administration for the entre chamber. The chamber is flexible so that the attached fiberscope could be adjusted vertically to focus on the subject. The upper part of the chamber locks onto the base with staggered metal groves for proper light tightness. The interior of the enclosure was fitted with externally operated LED lights for white light imaging which allowed seamless transition to CLI without having to move the setup.

The patient enclosure was constructed 360° around a clinical reclining chair with wooden panels which were lined with aluminum tape to obtain a light-proof material. The side panels had ports for both the CLI fiberscope and a panic button for the patient which were sealed with rubberized material to maintain lightproof operation. The enclosure was opened/closed using a double layered light blocking curtains which could be operated independently using an internal slide mechanism. The fiberscope could be positioned around the patient with a 3-finger mechanical arm.

Signal Uniformity of Efficiency of Curtain

100 ml of distilled water in a Petri dish containing 500μCi (18.5 MBq) of $^{68}GaCl_3$ was imaged and the surface plot was visualized (**Supplementary Figure 2a**). The efficiency of the curtains of the patient enclosure in blocking ambient light was determined by measuring CL with room lights both turned on and off (**Supplementary Figure 2b**).

Camera Linearity and Sensitivity to Exposure, Filters and Tissue Phantoms

The linearity and sensitivity were measured using $^{68}GaCl_3$ and ^{18}F-FDG in a black, opaque bottom 96-well plate which was cut in half to fit inside the animal enclosure. Serial dilutions were made in triplicate using 1X PBS to a final volume of 100 μL with each well containing 0, 1, 10, or 100μCi (0, 0.037, 0.37 or 3.7 MBq). Images were acquired using 60, 120 and 300 s exposure using the open filter. $^{223}RaCl_2$ sensitivity measurements were conducted with 37μCi (1.37 MBq) in 6mL of saline contained within a syringe and imaged for 5, 10, 30, 60, 120, and 300 seconds. Acquired images were filtered with a median filter (kernel size of 2x2 pixels), 20000 intensity cutoff to remove any remaining gamma strikes in ImageJ. Region of interest analysis was done in ImageJ, with mean intensity and variation reported over the exposure lengths for each isotope (**Supplementary Figure 3b, 3c**). Keeping exposure constant at 120 s, the dependence of CL

intensity on 0.78, 1.57, 3.13, 6.25, 12.5, 25, 50, or 100μCi (0.029, 0.058, 0.116, 0.231, 0.463, 0.925, 1.85 or 3.7 MBq) $^{68}GaCl_3$ was determined for 500 nm short-pass (SP), 525 nm bandpass (BP), 575 nm bandpass (BP) and 600 nm long-pass (LP) filters using region of interest analysis (**Supplementary Figure 3d**). Again, using 100μCi (3.7 MBq) $^{68}GaCl_3$ and a 120 s exposure time, the effect of open 1 or 2 bologna slices on the CL intensity were also determined for all the filters (**Supplementary Figure 3e**). Fiberscope scintillation tests were done with a ^{18}F-FDG source containing 337.8μCi (12.5 MBq) in 1cc and placed at 0, 1, 2, 3, 4, and 8 inches from the proximal end of the fiberscope with the attached lens capped and exposures were acquired over 300 seconds each.

Calibrated light source imaging was performed using a stabilized light source (L11494-660, Hamamatsu, Japan) set at 1.0 pW with a series of neutral density filters (NE-503B-A,506B-A,510B-A,513B-A,551B-A each housed in a respective LMR05 mount, Thorlabs, NJ, USA) under 4x4 and 8x8 binning for 15 and 5 minutes, respectfully. Lower light intensity images were acquired with the addition of neutral density filters to determine the detection limit of the system as 0.03 pW (**Supplementary Figure 4**). Resolution tests were performed with a luminescent resolution test target (Sighting Block B, LPA_00699_B) with 1x1, 4x4, and 8x8 binning modes (**Supplementary Figure 5**). Resolution profiles were measured using MATLAB (MATLAB 2019b, MathWorks, CA, USA) with the graphs generated in Prism (Version 9.1.0, GraphPad, CA, USA)

CLI Imaging of Mice with Intratumorally Injected Activity

Mouse studies were conducted with the approval of the MSKCC IACUC under the protocol of Dr. Jan Grimm. Nude mice from Jackson Laboratories bearing two HT1080 xenografts each, were injected intratumorally with 0, 12.8, 29.3, 55.1, 87.21, or 108.8μCi (0, 0.47, 1.08, 2.04, 3.06 and 4.03 MBq) ^{18}F-FDG in 20 μL PBS. CLI images were acquired using open filter for 300 s and overlaid with the white light image (**Supplementary Figure 6a**). CL intensity was calculated using region of interest analysis and plotted against injected activity (**Supplementary Figure 6b**). In a separate experiment, mice with HT1080 xenografts were intratumorally injected with 30μCi (1.11 MBq) $^{68}GaCl_3$ and imaged using different filters. The CL intensity was measured using region of interest analysis (**Supplementary Figure 6c**).

CLI Imaging of tissue phantom with filters

The tissue phantom was prepared using a combination of Agarose (BP160-500, Fisher Scientific, NJ, USA) dissolved in distilled water with the addition of India Ink for absorption (STIIN25, American MasterTech Scientific Inc, CA, USA or Bombay India Ink, Dr. Ph Martin's CO, USA) and Aluminum oxide for scattering (54483-50G, Sigma-Aldrich, MO, USA).[1] The solution was heated to 95°C with constant stirring on a hot plate before being poured into the 3D printed mold. The phantom was left to solidify overnight at 4°C. Five 3D printed spheres containing ~570μCi of clinical 18F-FDG each were prepared and embedded into the phantom at different depths. The tissue mimicking Agar removed to make the holes was remelted and poured into the hole with the sphere to ensure optical consistency throughout the phantom. When set, the phantom was transported to the hospital for CLI imaging and subsequently PET/CT imaging. CLI was carried out with 4x4 binning in EMCCD mode as previously described, for 15 minutes for each respective optical filter plus the open channel. PET/CT was acquired on a clinical GE Discovery PET/CT for 5 minutes and processed using the GE PACS system with activity analysis performed in HERMES software suite. CLI analysis was done using the macro as described previously, with a threshold setting of 93.5%.

References

1 Ntombela, L., Adeleye, B. & Chetty, N. Low-cost fabrication of optical tissue phantoms for use in biomedical imaging. *Heliyon* **6**, e03602 (2020).